PHYSICAL REVIEW B VOLUME 21, NUMBER 8 15 APRIL 1980

Extended muffin-tin orbital theory applied to the reaction of $CO+H_2$ on Ni(001)

R. V. Kasowski and Ed Caruthers
Central Research and Development Department, E. I. du Pont de Nemours and Company, Wilmington, Delaware 19898
(Received 31 July 1979)

The method using energy bands from a linear combination of muffin-tin orbitals has been extended so that the unit cell is now divided into muffin-tin and non-muffin-tin regions, instead of atomic Wigner-Seitz cells. The full potential including the nonspherical contribution to the potential is still included throughout the unit cell. The new method has been applied to the interaction of $CO + H_2$ on Ni(001) surface. Through use of three-dimensional charge-density plots, we show that CO forms $C + CO_2$ through disproportionation. We also show that the Ni(001) surface can break the carbon-oxygen bond of formaldehyde, but not carbon monoxide.

I. INTRODUCTION

The method using energy bands from a linear combination of muffin-tin orbitals (LCMTO)[1,2] has been revised in two important respects: First, the unit cell is now simply divided into muffin-tin regions and an interstitial region, instead of atomic Wigner-Seitz cells, and second, the muffin-tin-orbital wave function has been rewritten so that the charge density can be readily calculated. In fact, the charge density can be calculated so readily that we have implemented three-dimensional stereographic projection charge-density contour plots.[3] Such plots, as will be shown later in this paper, are useful in identifying the molecular bond that might break when the molecule is chemisorbed on a surface.

All the desirable features of the previous LCMTO method[1] have been retained. The nonspherical part of the potential is still included throughout the unit cell. Furthermore, two sets of muffin-tin orbitals[1] can be simultaneously included to improve the basis set and thus reduce the need to minimize the eigenvalues as a function of the muffin-tin-orbital-parameters energy E and plane-wave-tail dependence K^2. This feature is very useful for studying molecules on surfaces of thin films. Finally, the superlattice model[4,5] is employed to study molecules and chemisorption on surfaces. A hypothetical solid is composed of a periodic array of thin films, each separated by an open interval of several interatomic distances from the neighboring film. Such a superlattice is now in use by many investigators using different types of energy-band methods.[6,7]

In this paper, the extended muffin-tin orbital theory (EMTO) will be used to study the interactions of hydrogen, carbon monoxide, and formaldehyde with an Ni(001) surface. We will show that the CO triple bond does not break on Ni(001) for a variety of positions. However, we show that the CO bond can be broken by disproportionation of two CO molecules into CO_2 and a C atom. The disproportionation can occur either between two chemisorbed molecules or between a chemisorbed and a gas-phase CO molecule. Finally, we show that the formaldehyde carbon-oxygen double bond can break on Ni(001) at a bridge site with the CO axis parallel to the surface. The above results will be used to argue that Ni is a good methanation catalyst but a poor Fischer-Tropsch catalyst which is of course well established experimentally.[8]

In Sec. II, we describe the EMTO method as applied to bulk crystals or superlattices of molecules or thin films. Section III contains the three-dimensional charge-density plots for CO, formaldehyde, and acrolein. These molecules were chosen in order to illustrate bonding in typical organic compounds. Disproportionation of two CO's is calculated in Sec. IV. The surface dissociation of formaldehyde is shown in Sec. V. Section VI summarizes our findings on why Ni is a methanation catalyst.

II. EXTENDED EMTO THEORY

The EMTO theory will be presented in the same order that a calculation is performed. The first step is to overlap atomic charge densities to form a potential. Next muffin-tin spheres are drawn about each atom in the unit cell. The potential is divided into a muffin-tin part $V_{MT}(r)$ and a non-muffin-tin part $\Delta V(r)$. $\Delta V(r)$ is defined throughout the unit cell including inside the muffin-tin spheres.

Muffin-tin orbitals $\chi_{lm}(E_1, K, r, \tau)$ are next constructed from radial solutions $\phi_{lm}(E_1, \vec{r}, \vec{\tau})$ of the muffin-tin potential at fixed energy E, for each atom $\vec{\tau}$ in the unit cell:

$$\chi_{lm}(E_1,K_1,\vec{r},\tau)=\phi_{lm}(E_1,\vec{r},\vec{\tau})+C_l(E_1,K_1)\bar{J}_{lm}(K_1,\vec{r},\vec{\tau}),\quad r\le S$$
$$=-S_l(E_1,K_1)\bar{K}_{lm}(K_1,\vec{r},\vec{\tau}),\quad r\ge S. \quad (1)$$

C_l and S_l are determined by continuity of the logarithmic derivative at the muffin-tin sphere radius S. $\bar{J}_{lm}(K_1,\vec{r},\vec{\tau})$ is that solution, $J_{lm}(K_1,\vec{r}_1,\vec{\tau})$ of the wave equation at energy K_1^2, which is orthogonalized to the core states of the potential at atom $\vec{\tau}$, while $\bar{K}_{lm}(K_1,\vec{r},\vec{\tau})$ is a solution which is orthogonalized to the core states on all other sites. J_{lm} and K_{lm} are defined as products of spherical-harmonic and spherical Bessel and Neumann functions such that they are regular at the origin and at infinity, respectively.

MTO-Bloch functions are formed for the fixed parameters E_1 and K_1^2.

$$\chi^{\vec{k}}_{lm}(E_1,K_1,\vec{r},\vec{\tau})=\sum_n e^{i\vec{k}\cdot\vec{R}_n}\chi_{lm}(E_1,K_1,\vec{r},\vec{\tau}). \quad (2)$$

The variational principle is next used to solve the Schrödinger equation

$$\langle\chi^{\vec{k}}_{l_1m_1}(E_1,K_1,\vec{r},\vec{\tau}_1)|H-E|\chi^{\vec{k}}_{l_2m_2}(E_2,K_2,\vec{r},\vec{\tau}_2)\rangle=0. \quad (3)$$

Fixed MTO-parameters are E_1,K_1,E_2,K_2 to indicate the possibility of two sets of MTO's per atom $\vec{\tau}$.

The Hamiltonian is divided into muffin-tin and interstitial regions

$$\langle\chi^{\vec{k}}_1|H-E|\chi^{\vec{k}}_2\rangle=\langle\chi^{k}_1|-\nabla^2+V_{MT}-E|\chi^{k}_2\rangle_{MT's}+\langle\chi^{k}_1|\Delta V|\chi^{k}_2\rangle_{MT's}+\langle\chi^{k}_1|-\nabla^2+\Delta V-E|\chi^{k}_2\rangle_{interstitial}. \quad (4)$$

The abbreviation MT's indicates integration over the muffin-tin volumes and interstitial indicates integration over the interstitial region. $\chi^{\vec{k}2}_1$ is defined to be the Bloch function with parameters l_1, m_1, E_1, K_1^2, and $\vec{\tau}_1$. A similar definition holds for $\chi^{\vec{k}}_2$.

We next add and subtract the muffin-tin terms

$$\langle\chi^{\vec{k}}_{j_1}|K_2^2+\Delta V-E|\chi^{\vec{k}}_{j_2}\rangle$$

where χ_j is a pseudo-wave-function which satisfies

$$\chi_{j_1}=\begin{cases}J_l(K,\vec{r})+C_l\dfrac{dJ_l}{dE}, & \vec{r}\le S\\ -K_l, & \vec{r}\ge S.\end{cases} \quad (5)$$

C_l ensures continuity of χ_j and its derivatives at S. dJ_l/dE is the energy derivative of the Bessel function J_l.

We find that to a good approximation,

$$\langle\chi^{\vec{k}}_1|\Delta V|\chi^{\vec{k}}_2\rangle-\langle\chi^{\vec{k}}_{j_1}|\Delta V|\chi^{\vec{k}}_{j_2}\rangle\approx 0, \quad (6)$$

because $\chi_{j_1}=\chi_2$ at the muffin-tin radius, and inside the MT's, ΔV approaches zero as $\chi^{\vec{k}}_1$ deviates from $\chi^{\vec{k}}_{j_1}$.

The Hamiltonian can now be written as

$$\langle\chi^{\vec{k}}_1|H-E|\chi^{\vec{k}}_2\rangle=\langle\chi^{\vec{k}}_1|\nabla^2+V_{MT}-E|\chi^{\vec{k}}_2\rangle_{MT's}-(K_2^2+V_{MTZ})\langle\chi^{\vec{k}}_{j_1}|\chi^{\vec{k}}_{j_2}\rangle_{MT's}+\langle\chi^{k}_1|K_2^2+\Delta V-E|\chi^{k}_{j_2}\rangle_{interstitial}+\langle\chi^{k}_{j_1}|K_2^2+V_{MTZ}+\Delta V-E|\chi^{k}_{j_2}\rangle_{MT's}. \quad (7)$$

V_{MTZ} is the muffin-tin constant so that ΔV is not discontinuous at S. The first two terms are done easily by the usual LCMTO formalism, as only the spherical part of the potential is used. The second two terms are done by numerical integration as the integrand ΔV is smoothed over the entire unit cell. In performing the numerical integration, we generate the true wave function on a random set of points. This tabulated wave function is saved and used after solution of the Hamiltonian to calculate charge density for display purposes. In future calculations, the charge density will be iterated to self-consistency. This extended muffin-tin-orbital theory could also be used with linearized MTO's[9] instead of the orthogonalized MTO's used here.

Relativistic corrections (without spin orbit)[10] are also included in our Hamiltonian. The starting potential is formed by overlapping relativistic charge densities obtained from the Liberman, Waber, and Cromer[11] program. The exchange parameter was chosen to be $\alpha=1.0$ for the calculations in this paper.

Finally, we illustrate in Table I how molecular eigenvalues depend on the different parameters involved in MTO calculations. For CO adsorbed vertically on a four-fold site of Ni(001), C-to-Ni distance = 1.90 Å, we show E_F and five bonding CO molecular-orbital energies at the Γ point. This table illustrates that all the molecular-orbital energies pass through a minimum near $K^2=-0.4$ Ry. This negative value of K^2 gives a decaying tail to the MTO basis functions which is necessary for fitting the localized molecular levels. The effect of the energy parameters E_i is much less than the effect of K^2. Finally, as discussed in Ref. 1, the Ni d states are approximately independent of K^2, and vary much more slowly than the molecular orbital levels shown

TABLE I. Molecular energies as a function of muffin-tin-orbital parameters.

K^2 (Ry)	−0.8	−0.4	−0.15	0.15	0.5	−0.4	−0.4
E_s (eV)	−21.76	−21.76	−21.76	−21.76	−21.76	−17.68	−17.68
E_p (eV)	−17.68	−17.68	−17.68	−17.68	−17.68	−13.60	−13.60
E_d (eV)	−10.88	−10.88	−10.88	−10.88	−10.88	−6.80	−6.80
α	1.0	1.0	1.0	1.0	1.0	1.0	0.667
3σ (eV)	−35.12	−35.71	−30.227	−24.93	−20.13	−33.69	−30.37
4σ (eV)	−20.14	−21.69	−20.60	−20.19	−18.87	−20.83	−17.83
5σ (eV)	−17.21	−18.44	−17.21	−15.20	−11.00	−17.86	−14.39
π (eV)	−14.96	−17.04	−16.83	−16.80	−16.13	−16.17	−12.5
E_F (eV)	−8.61	−8.68	−8.61	−8.60	−8.2	−8.61	−4.92

here. Thus, the MTO parameters in column two ($K^2 = -0.4$ Ry) were used throughout this paper for chemisorption calculations. We add that the effect of α is to roughly shift all eigenvalues by approximately 3 eV. $\alpha = 1.0$ has been chosen here as this value tends to give better band structures for non-self-consistent calculations on metals.

III. APPLICATION OF EMTO TO CO, H_2CO, AND C_3H_4O

The EMTO formalism is applied to molecules by forming a superlattice composed of molecules spaced far apart so as not to interact with each other. For CO, we form a planar arrangement of CO corresponding to the $C(2\times2)$ structure observed on Ni(001). The planes of CO molecules are separated by a vacuum region equivalent to four layers of Ni(001). The same superlattice was also used for H_2CO, whereas a much larger superlattice was required for C_3H_4O.

CO, H_2CO, and C_3H_4O were studied here to provide pictures of bonding often encountered in organic compounds: C-H, C-C, C=C, C=O, and C≡O. In the following sections, we will determine under what conditions these different bonds can break on Ni(001).

In Fig. 1, the eigenvalues calculated with the EMTO method are compared to the measured ionization potentials for CO, H_2CO, and C_3H_4O.[12] There is a good overall agreement between the calculated eigenvalue spectrum in columns labeled (a) and the ionization potentials in columns (c) even though all three calculations were performed with a minimal MTO basis set consisting of only one set of MTO's per atom. For these MTO's the tail parameter K^2 was set equal to −0.4 Ry and the MTO energy parameter was set equal to −1.1 Ry for s functions and −0.6 Ry for p functions. The agreement with experiment is improved if another set of MTO's with $K^2 = 0.5$ Ry is included in the basis set. These results are given in Fig. 1 under columns (b).

In Fig. 2, we compare three-dimensional valence charge density plots for CO, H_2CO, and C_3H_4O. These plots are stereographic projections of a three-dimensional closed contour of constant charge density.[13] Here the closed-contour value is 0.1 electrons/a.u.^{3}. The closed three-dimensional contour is represented by sets of closed two-dimensional contours in perpendicular planes.

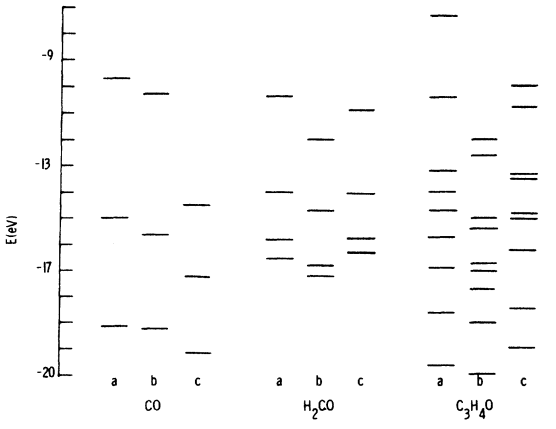

FIG. 1. Comparison of electronic energy levels calculated for CO, H_2CO, and C_3H_4O with results for small basis set in columns (a) and large basis set in columns (b). The ionization potentials are given in columns (c).

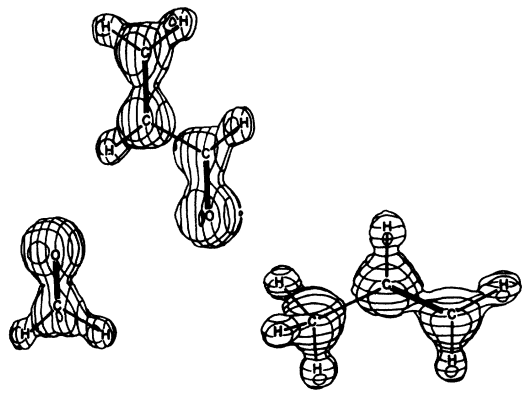

FIG. 2. Plots of the total charge density contour ($=0.1e$/a.u.^{3}) for CO, H_2CO, and C_3H_4O.

The closed contour (=0.1 e/a.u.^{3}) encloses about 90% of the total charge.

Figure 2 shows that the total valence charge goes through a minimum along each bond. The amount of charge at a minimum depends on the number of electrons in the bond and on the bond length. Thus, the minimum along C=O is greater than the minimum along C=C, because C=O is the shorter bond. The charge along C-C shows a gap, but the charge does not go to zero. It is merely less than 0.1 e/a.u.^{3}.

Two points about these calculations deserve special emphasis. First, a minimal MTO basis set allows accurate calculation of both valence eigenvalues and total valence charge densities. Second, our two-dimensional projections of three-dimensional valence-charge-density contours allow a very clear visualization of different kinds of molecular bonding. These two points will be exploited in our calculations of molecule-surface interactions.

IV. INTERACTION OF CO MOLECULES ON Ni

It is well established that CO gas in the presence of Ni at 140 °C leads to deposition of carbon and the formation of CO_2.[13] We have investigated three different reaction routes that might account for this experimental observation. First, a CO molecule could dissociate into C plus O. The O atom could then react with a CO molecule to form CO_2:

$$CO \rightarrow C + O, \quad CO + O \rightarrow CO_2. \tag{8}$$

A second possibility is that a gas-phase CO molecule interacts with a chemisorbed CO to form CO_2 plus C:

$$CO(\text{adsorbed}) + CO(\text{gas}) \rightarrow CO_2 + C. \tag{9}$$

The third possibility investigated is that two chemisorbed CO's interact to form CO_2+C:

$$CO(\text{adsorbed}) + CO(\text{adsorbed}) \rightarrow CO_2 + C. \tag{10}$$

The mechanism in Eq. (9) is often called Ely-Rideal[14] (ER), whereas the mechanism in Eq. (10) is called Langmuir-Henschelwood (LH).

One difficulty in studying the interaction of molecules at a surface is that surface interatomic bond distances are unknown. As a result we have chosen bond distances from comparable solids and molecules. For example, the Ni-C distance was chosen to be that of $Ni(CO)_4$ (1.84 Å) for calculations where the C atom is close to the surface. The smallest possible Ni-O distance was chosen to be that in NiO (2.09 Å). The C-O distance was maintained at its molecular value.

In order to investigate the dissociation of CO via Eq. (8) the electronic properties of CO adsorbed onto Ni were calculated for a variety of positions. The surface structure used was $C(2\times2)$. The calculations were performed with a superlattice model consisting of three-layer films of Ni(001) separated by five-layer-thick vacuum regions. Molecules are placed on only one side of the film. The surface structure is $C(2\times2)$ as found by low-energy-electron diffraction LEED for CO on Ni(001). In Fig. 3, the charge density contours are shown for a top position, a bridge position, a four-fold hollow position, and parallel to the surface. The value of the charge density chosen for the contour is 0.1 e/a.u.^{3} as discussed in the previous section. For clarity, only the surface layer Ni atoms are included in the plots.

The charge density contour plots in Fig. 3 show no evidence that the CO bond has broken. The CO charge density contours resemble closely that of the free CO molecule in Fig. 2. Thus, our calculations suggest direct dissociation of CO on Ni(001) is unlikely, and the mechanism in Eq. (8) may not occur monomolecularly.

We next investigate the Ely-Rideal mechanism of Eq. (9). For these calculations, we assume that the gas-phase CO interacts linearly with the chemisorbed CO in the four-fold hollow, as previously proposed by Anderson *et al.*[16] In Fig. 4, the resultant charge density contours are plotted. The first contour [Fig. 4(a)] shows the interaction of two CO molecules with the C-Ni distance being that of $Ni(CO)_4$ and the C-O distance between molecules being that of CO_2. One clearly sees that a CO_2 molecule has started to form in that charge is pulled away from the C atom and

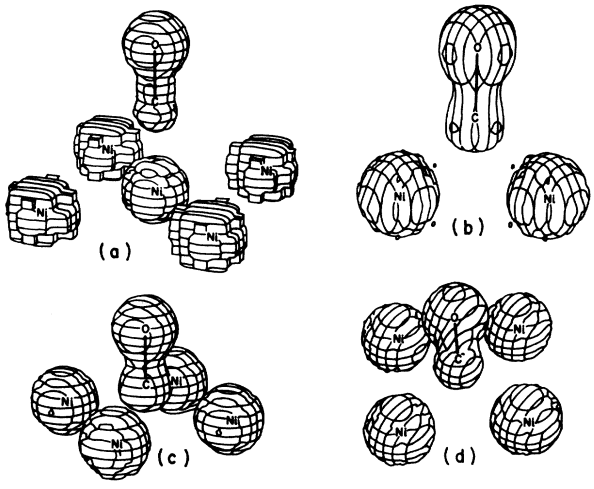

FIG. 3. Charge-density plot for CO on Ni(001) at a (a) top position, (b) bridge position, (c) four-fold hollow, and (d) parallel to the surface.

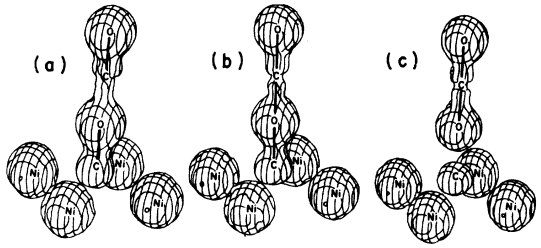

FIG. 4. Charge-density plot showing the disproportionation of a gas-phase CO molecule with a chemisorbed CO on Ni(001).

donated to its neighboring O atoms, as is characteristic of free CO_2.

Next, the carbon-oxygen distances were increased to those found in CO_2. The contour in Fig. 4(b) shows that the bond between the surface carbon and the oxygen-carbon-oxygen molecule has begun to break, since CO_2 appears to have formed. The last step is to raise the CO_2 molecule from the surface carbon atom. In Fig. 4(c), the CO_2 molecule has been raised 0.2 Å above the surface. Note the similarity of the CO_2 charge density in the three contours in Fig. 4. The importance of bond stretching to the disproportionation suggests that this is an activated process and helps rationalize the need for high temperatures (140 °C).

We have found that the same disproportionation reaction can occur on Ni(110). The three plots corresponding to those of Fig. 4 are shown in Fig. 5. It appears to make little difference that a bridge site was chosen to chemisorb the CO molecule on the (110). We expect that disproportionation via Eq. (9) can occur at a variety of sites. Thus, these results support the model proposed by Anderson *et al.*[15]

Finally, we show that disproportionation can occur between two chemisorbed molecules as in Eq. (10). The $c(2\times2)$ surface unit cell used in the previous calculations is too small to allow

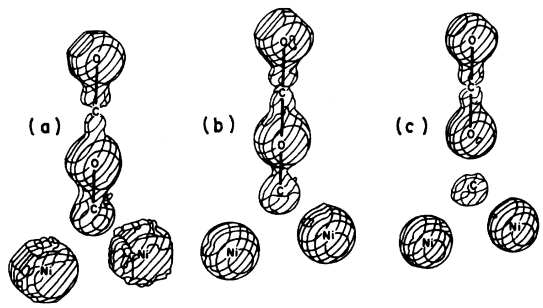

FIG. 5. Charge-density plot showing the disproportionation of a gas-phase CO with a chemisorbed CO on Ni(110).

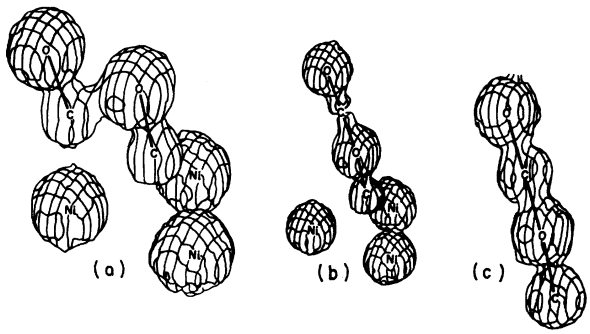

FIG. 6. Charge-density plot showing disproportionation of two chemisorbed CO molecules on Ni(111).

two chemisorbed molecules to interact without overlapping strongly with neighboring CO's. Thus, we switched to a (111)-symmetry film which is three layers thick and has a $\sqrt{3}\times\sqrt{3}R30°$ surface pattern, i.e., three Ni atoms for each layer in the unit cell. This unit cell is large enough so that two chemisorbed molecules interact strongly with each other, but only weakly with neighboring chemisorbed molecules.

In Fig. 6, we show a sequence of charge-density plots that suggest that disproportionation is possible between two chemisorbed molecules. In Fig. 6(a), one CO is placed in the three-fold hollow, tilted at an angle of 30° from normal. The second CO is at a top site at an angle of 30° from normal. The C-Ni distances are those of $Ni(CO)_4$. The carbon oxygen distances are those of CO_2. In Fig. 6(b), we assume that the C-Ni bond is broken resulting in a linear C-O-C-O molecule. This charge density contour suggests that a CO_2 molecule has formed. It appears this reaction requires activation to bend the molecules away from normal, to break the C-Ni bond and to release the CO_2 molecule.

The importance of the Ni substrate is crucial to the formation of CO_2. In Fig. 6(c), the charge-density contour for a C-O-C-O molecule in the absence of an Ni substrate is plotted. There appears to be no evidence of CO_2 formation when the Ni substrate is absent.

Thus, it appears that kinetic studies are required in order to distinguish whether ER or LH is the predominant mechanism by which CO_2 is formed on Ni.

V. DISSOCIATION OF FORMALDEHYDE ON Ni(001)

As already discussed in Sec. III, formaldehyde contains a C-O double bond. In this section, we show that this C-O bond can be broken at a special site on Ni.

In Fig. 7, charge density contours have been

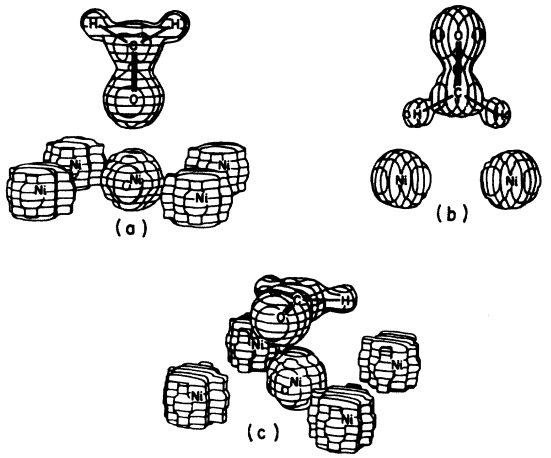

FIG. 7. Charge-density plot for formaldehyde interacting with a Ni(001) surface.

plotted for H_2CO interacting with (100)Ni for three positions: (a) top site, (b) bridge site, and (c) parallel top site. There is no evidence of bond breaking of either the C-H or the C-O for these positions. Figure 7 can also be used to support the hypothesis that $CO+H_2$ can form formaldehyde on Ni.

In Fig. 8, we show that the C-O double bond can be broken by putting the molecule flat on the surface at a bridge site. The Ni-H distance is that of NiH and the Ni-O distance is just a little more than that in NiO. One would expect the CH_2 fragment to form methane readily in the presence of H_2. Thus, any formaldehyde formed on Ni can be changed to methane.

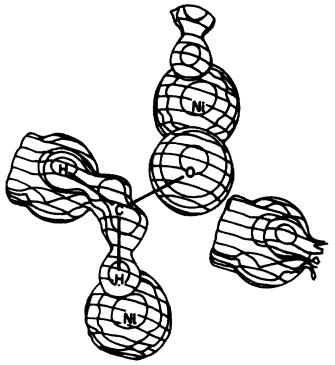

FIG. 8. Charge-density plot showing that the carbon-oxygen bond of formaldehyde is broken if the molecule is flat on the Ni(001) surface at a bridge site.

The first mechanism of formation of CH_4 is disproportionation of CO either by Ely-Rideal or Langmuir-Henschelwood:

$$CO+CO \rightarrow CO_2+C, \tag{11}$$

$$C+2H_2 \rightarrow CH_4. \tag{12}$$

The second mechanism involves formation of formaldehyde and then bond breaking:

$$2H+CO \rightarrow H_2CO, \tag{13}$$

$$H_2CO \rightarrow H_2C+O, \tag{14}$$

$$H_2C+H_2 \rightarrow CH_4. \tag{15}$$

Thus, the production of higher hydrocarbons is circumvented.

VI. SUMMARY

The Fischer-Tropsch process involves the production of hydrocarbons from CO and H_2 over a metal catalyst. It is commonly suggested, although unproved, that formaldehyde is an intermediate in the Fischer-Tropsch process.[8] Ni is a poor Fischer-Tropsch catalyst. Our results provide insight into the mechanisms by which CH_4 might be produced over Ni.

ACKNOWLEDGMENTS

The authors wish to thank Dr. H. S. Jarrett for many useful discussions. We also wish to thank Dr. D. Pensak for making available to us the three-dimensional contour-plotting package and also explaining its use. Finally, we thank Dr. D. Papaconstantoupolos and Dr. B. Klein for giving us programs to calculate relativistic solutions of the Schrödinger equation.

[1]R. V. Kasowski, Phys. Rev. B 14, 3398 (1976).
[2]O. K. Andersen and R. V. Kasowski, Phys. Rev. B 4, 1064 (1971).
[3]L. Salem and W. Jorgensen, *The Organic Chemists Book of Orbitals* (Academic, New York, 1973). Original plotting package revised by D. Pensak.
[4]G. P. Alldredge and L. Kleinman, Phys. Rev. Lett. 28, 1264 (1973).
[5]S. G. Louie, K. M. Ho, J. R. Chelikowsky, and M. L. Cohen, Phys. Rev. B 15, 5627 (1977).
[6]J. G. Gay, J. R. Smith, and F. J. Arlinghaus, Phys. Rev. Lett. 38, 561 (1977).
[7]E. E. Lafon and C. C. Lin, Phys. Rev. 152, 579 (1966); S. Ciraci and I. P. Batra, Phys. Rev. B 15, 3254 (1977); W. Y. Ching and J. Callaway, *ibid.* 9, 5115 (1974).
[8]M. A. Vannice, Catal. Rev. Sci. Eng. 14, 153 (1976).
[9]O. K. Andersen, Phys. Rev. B 12, 3060 (1975).

[10]D. D. Koelling and B. N. Harmon, J. Phys. C 10, 3107 (1977).
[11]D. Liberman, J. T. Waber, and D. T. Cromer, Phys. Rev. 137, A27 (1965).
[12]D. Turner, C. Baker, A. Baker, and C. Brundle, *Molecular Photoelectron Spectroscopy* (Wiley-Interscience, New York, 1970).
[13]J. C. Bertolini and B. Imelik, Surf. Sci. 80, 586 (1979).
[14]K. Tamaru, *Dynamic Hetergeneous Catalysis* (Academic, London, 1978).
[15]S. Andersson, in Proceedings of the Seventh International Vacuum Congress and Third International Conference on Solid State Surfaces, Vienna, 1977, p. 1019 (unpublished).